Available online at www.sciencedirect.com

ScienceDirect

Energy Procedia 105 (2017) 3990 – 3996

Energy Procedia

The 8th International Conference on Applied Energy – ICAE2016

Performance Enhancement of Battery Charger for Electric Vehicles Using Resonant Controllers

Liwen Pan[a, *1], Chengning Zhang[a]

[a] National Engineering Laboratory for Electric Vehicles, Beijing Institute of Technology, Beijing, 100081, China

Abstract

This paper proposes a current proportional-resonant control strategy to reduce second-order harmonic of electric vehicle battery charger. Using the PR controller, the charger reference tracking performance can be enhanced. The steady-state errors in single-phase charging system can be reduced effectively. The PR controller stability influence factors including proportion coefficient, resonant coefficient and cutoff frequency are discussed in the paper. Finally, simulation results achieved on a 3.3kW charging model prove the proposed strategy effectively minimizes the low-order frequency ripple in grid-interfaced converter.

Peer-review under responsibility of the scientific committee of the 8th International Conference on Applied Energy.

Keywords: Electric vehicle charger, proportional-resonant controller, ripple reduction

1. Introduction

The development of electric vehicles (EVs) battery charger system has received much more attention in research communities, auto-manufacturers and government [1-4]. EV charger is a kind of power converter which performs electric energy from the grid to energy storage device. It is an essential element between the grid and EVs battery pack. Furthermore, the battery charger is highly non-linear load in power system. It presents a potential problem to grid in forms of poor power factor and excessive harmonic current injection. It imposes a requirement on the battery charger not only charger the battery efficiently but also follow IEEE 1547 standard.

A variety of circuit topologies have been developed for EV battery charger. The two-stage ac/dc and dc/dc power conversion architectures is considered as suitable for EV battery charger. However, the single phase ac/dc converter provides inherent low frequency ripple in grid current. A large dc link capacitor is used to filter the input power fluctuation. Unfortunately, the electrolytic capacitor cannot be used for EV application due to its short lifetime. A film capacitor is selected to replace electrolytic capacitor, which results in an increasing of the size and cost of the converter device. High power density is crucial for on-board battery charger of EV due to the space constraints. With the development of wide bandgap power electronic switches, Silicon Carbide (SiC) and Gallium Nitride (GaN) are used in EV battery charger application gradually, which can improve the system switching frequency effectively. However, the ripple energy at twice the grid frequency cannot be reduced by increasing the switching frequency.

Typical EV battery charger consist of an input filter, an EMI filter, a bidirectional rectifier, a power factor correction circuit and isolated dc/dc converter. The general block diagram of an EV battery charger described above can be seen in Fig.1.

[1] * Liwen Pan. Tel: +86-156-529-9974; fax: +86-010-6891-2947.
E-mail address: panliwen2002@163.com.

Peer-review under responsibility of the scientific committee of the 8th International Conference on Applied Energy.
doi:10.1016/j.egypro.2017.03.835

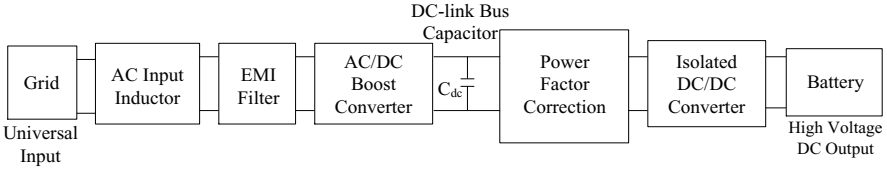

Fig.1. Typical block diagram of an EV battery charger.

Regarding single phase battery-charging system, the battery is subject to current ripple which is two times of the line frequency. Some Lithium Iron Phosphate battery test results indicate the low frequency current ripple such as double frequency ripple cause noticeable battery temperature increasing. The performance of Lithium ion battery do not deteriorate significantly with high frequency harmonic current. Therefore, further investigation is still needed to research about the low frequency current ripple effect based on repetitive cycle tests over a long term.

The bidirectional rectifier can boost the grid voltage and regulate it to dc link. The conventional ac/dc boost converters use a simple linear proportional-integral (PI) controller, which includes steady-state error in single phase system. The proportional-resonant (PR) controller is proposed in this paper to improve the EV battery charger performance.

The paper is organized as follows: the EV grid-connected charger system configuration is briefly recalled in Section 2. In Section 3 the single phase rectifier passive components are designed. Based on the circuit parameters, the PR controller impact on ripple energy at twice line frequency is analyzed and investigated in Section 4. Section 5 shows the simulation results to verify the proposed PR control strategy. The conclusion is presented in Section 6.

2. EV battery charger system configuration

The topology of the single phase PWM rectifier is described in Fig.2. u_{ac} and i_{ac} represent the grid voltage and current, respectively. U_{dc} and I_{dc} represent the load voltage and current. The unipolar modulation method is shown in Fig.3.

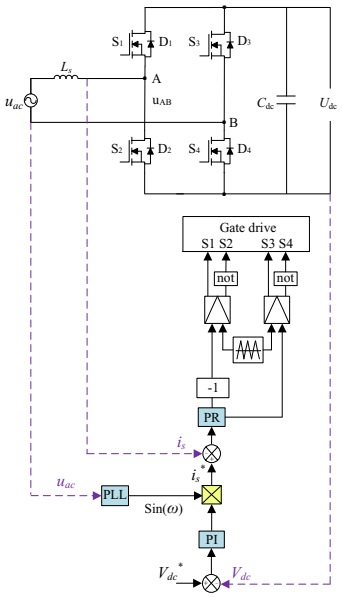

Fig.2. Single-phase PWM rectifier topology structure.

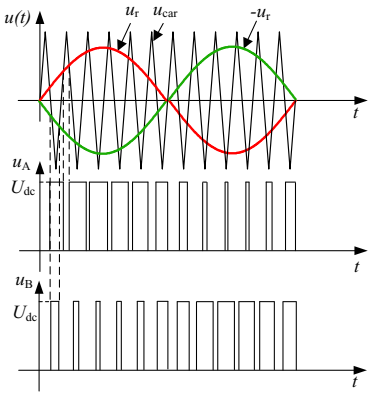

Fig.3. Unipolar modulation.

The vector relationship between grid side electromotive force E, grid voltage V, input inductor voltage V_L and grid current I_{ac} can be seen in Fig.4.

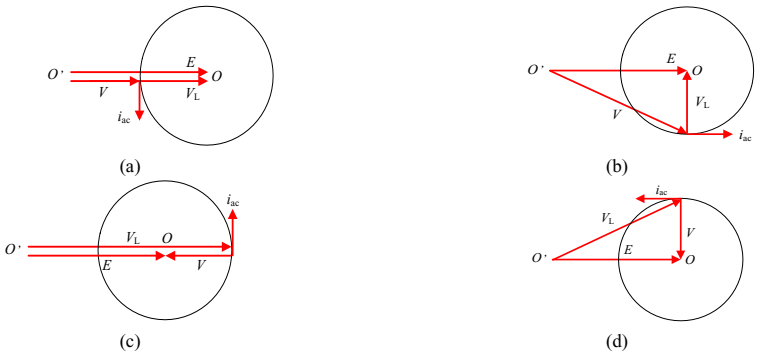

Fig. 4. Vector relationship: (a) Inductance property; (b) Positive resistance property; (c) Capacitance property; (d) Negative resistance property.

Based on the above vector relationship analyzation, the single phase rectifier PWM modular system is able to be operated on all four-quadrants, as shown in Fig.5.

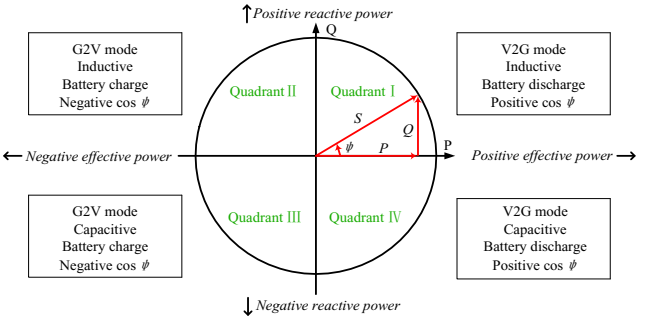

Fig.5. Single phase rectifier PWM control in all four-quadrants.

Unipolar modulation is selected to control the single phase PWM rectifier for EV charger. Table 1 describes unipolar modulation in three operative modes.

Table1 Unipolar modulation in three operative modes.

Switching state	1	2	3	4
Conduction device	S1(D1), S4(D4)	S2(D2), S3(D3)	S1(D1), S3(D3)	S2(D2), S4(D4)
U_{AB}	U_{dc}	-U_{dc}	0	0

The unipolar modulation process can be described in Fig.6.

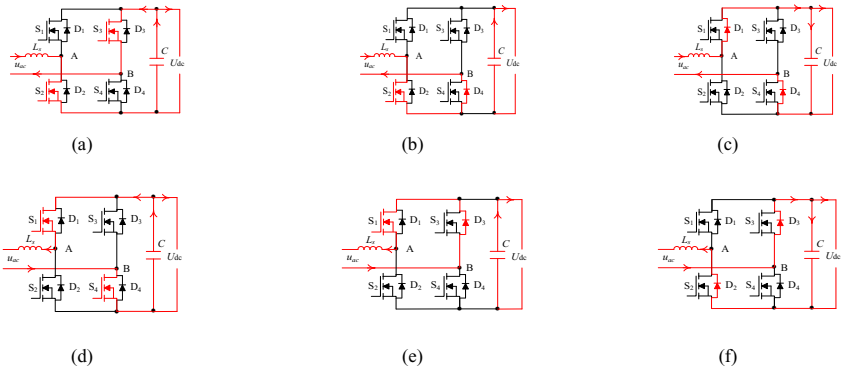

Fig.6. Unipolar modulation process: (a) Capacitor charge load, grid and capacitor charge inductor; (b) Capacitor charge load, grid charge inductor; (c) Grid and inductor charge capacitor and load; (d) Capacitor charge load and inductor; (e) Capacitor charge load; (f) Grid and inductor charge capacitor, inductor charge load.

3. Grid-connected converter passive components design

A large dc bus capacitor is needed to smooth the second order ripple on the dc side. Capacitor is considered as an energy buffer between input ac power and output dc power. Therefore, the capacitance can be selected based on the stored energy. The dc bus voltage ripple cannot exceed 2% of the dc link voltage in this paper. Meanwhile, in order to stabilize the dc output voltage, the capacitance usually leave some margin.

$$C_{dc} \geq \frac{P_o}{2\omega\sigma U_{dc}^2} \tag{1}$$

Where, P_o is output power, ω is the ac side angular frequency and σ is the ripple voltage ratio.

The input inductor is designed based on the current ripple on the inductor. It is assumed no grid wire and input inductor equivalent resistances exist. The single-phase PWM rectifier equation is given as followed:

$$\frac{di_s}{dt} = \frac{u_s - u_{AB}}{L_s} \tag{2}$$

Equation (3) shows the input inductor current.

$$\Delta i_s = T_s \frac{u_s - u_{AB}}{L_s} \tag{3}$$

Where, T_s is power switch device turn-on or turn-off time in a cycle time.

When actual current tracking reference current during each switching cycle, the amplitude of current fluctuation cannot exceed the required maximum peak current ripple. The amplitude of grid current fluctuation is limited within 10% of the peak current in this paper.

$$\frac{\left(U_{dc}^2 - U_{\max}^2\right)T_s}{2\Delta i_{\max} U_{dc}} \leq L_s \leq \frac{U_{dc} T_s}{\Delta i_{\max} \sin\left(\omega t\right)} \tag{4}$$

Where, $\Delta i_{\max}$ is the grid current maximum fluctuation and $U_{\max}$ is the ac side peak voltage.

4. PR control scheme

PR Controller can produce an infinite gain at the selected resonant frequency to eliminate steady state error at that frequency [5-6]. With the flexibility of tuning the resonant frequency, it is possible to filter low-order harmonic by selecting proper resonant frequency [7].

The ideal resonant controller transfer function can be expressed as:

$$G(s) = K_p + \frac{2K_r s}{s^2 + \omega^2} \tag{5}$$

Where, K_p represents proportional coefficient， K_r is resonance coefficient and ω represents fundamental angular frequency.

The ideal PR controller Bode plot is illustrated in Fig. 7 (a). As can been seen, the ideal PR controller has an infinite gain at the line frequency of ω, and no gain at other frequencies. To avoid stability problem associated with an infinite gain, transfer function (6) can be used instead of (5) to give a non-ideal PR controller [8].

$$G(s) = K_p + \frac{2K_r \omega_c s}{s^2 + 2\omega_c s + \omega^2} \tag{6}$$

Where, ω_c is cutoff frequency.

The non-ideal PR controller is illustrated in Fig.7 (b). As can been seen the gain is finite, but still relatively high to enforce small steady-state error. Meanwhile, the bandwidth is widen by setting ω_c appropriately, which is helpful for reducing sensitivity towards frequency variation [9]. It is shown in equation (6), the parameters K_p， K_r and ω_c effect on the performance of PR controller.

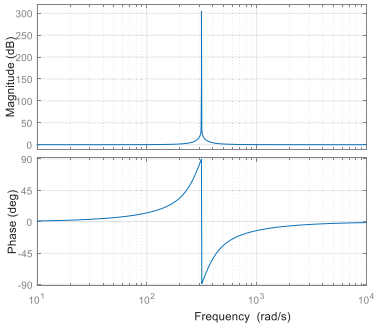

(a) K_p=1, K_r=100, ω=314 rad/s

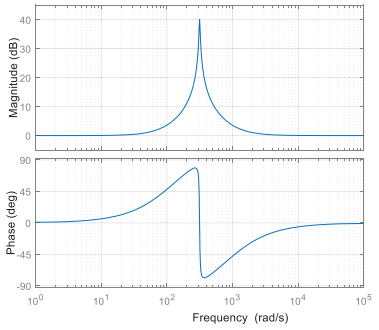

(b) K_p=1, K_r=100, ω=314 rad/s, ω_c=5 rad/s

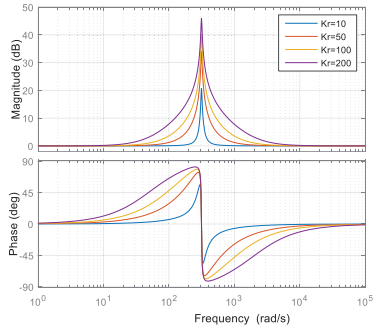

(c) K_p=1, ω_c=5 rad/s

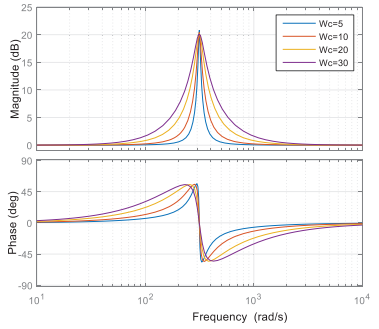

(d) K_p=1, K_r=10

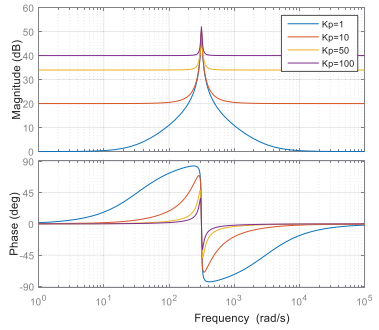

(e) K_r=300, ω_c=5 rad/s

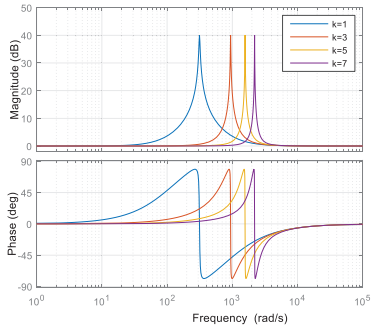

(f) K_p=1, K_r=100, ω_c=5 rad/s

Fig.7. PR controller Bode plot: (a) Ideal PR controller; (b) Non-ideal PR controller; (c) K_r performance; (d) ω_c performance; (e) K_p performance; (f) Specific harmonic frequency k performance.

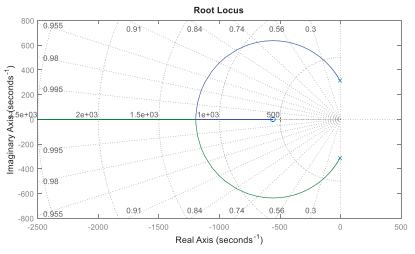

Fig.8. Root locus. (ω0=314, ωc=5)

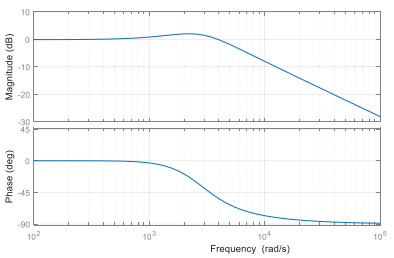

Fig.9. System Bode plot.

In Fig.7 (c), the gain at resonant frequency is increasing with resonant coefficient, but no effect on the

bandwidth. The range of frequencies can be widened with K_r increasing. Therefore, the undesirable frequency signal is amplified, the stability of system is reduced. The frequency response for different values ω_c is given in Fig.7 (d), the resonance frequency gain remains constant with cutoff frequency increasing while the system bandwidth is widened. Consequently, cutoff frequency determines the bandwidth. The frequency response for proportion coefficient is shown in Fig.7 (e). Obviously, the system gain increases with K_p, but the gain at resonant frequency remains stable. Therefore, K_p mainly have an influence at non-resonant frequency performance. Appropriate K_p can make the system better in terms of interference rejection. The multiple Bode plot is shown in Fig.7 (f). As can be seen, the gain at fundamental and 3, 5, 7 times specific harmonic frequency point are maximum. Consequently, the application of multiple PR controller can compensate the low order harmonic selectively.

The root locus of open-loop transfer function after pole-zero elimination of closed-loop transfer function is given in Fig.8. The root locus indicates the system can track the sinusoidal reference signal accurately [10]. The system Bode plot is shown in Fig.9. Fig.9 shows -3db is corresponding to the crossover frequency 5700rad/s. The high frequency harmonic at switching frequency can be filtered.

5. Simulation verification

The proposed PR controller is applied to a 3.3kW EV battery charger to test its feasibility and validity. The parameters of the battery charger is given in Table 2. The control scheme for the on-board single-phase battery charger is described in Fig.1.

Table 2 Single phase battery charger parameters.

Item	Value	Item	Value
Rated input voltage	220 V	DC link bus voltage	336±2% V
AC input frequency	50 Hz	DC link bus capacitor	2.33 mF
Input inductor	1.7 mH	Switching frequency	20 kHz

Fig.10 show the grid voltage and current simulation results under PI and PR control strategies, respectively. Fig.10 (a) and (b) show the voltage and current waveform of the ac side under PI and PR controller, respectively. It should be noted that, the error of ac current reduces almost 50% of original values under PR control.

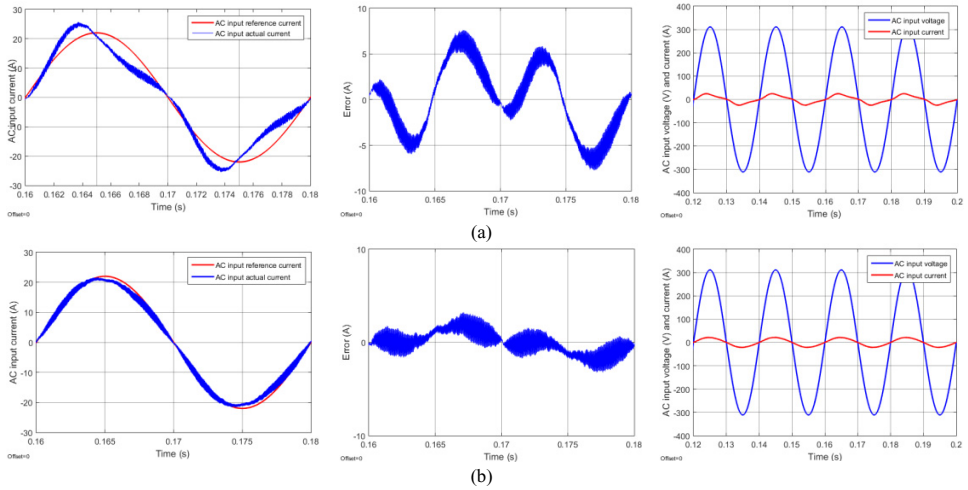

Fig.10. Simulation results: (a) PI; (b) PR.

It can be seen in Fig.11, the total harmonic distortion (THD) is 5.13% based on PI controller. The THD is only 1.92% based on PR controller. The simulation results show PR controller can reduce grid current harmonic components effectively.

(a) (b)

Fig. 11. FFT analysis: (a) THD result based on PI controller; (b) THD result based on PR controller.

6. Conclusion

In this paper, a current PR control strategy have been proposed for EV battery charger to reduce second-order harmonic current and corresponding ripple voltage on the dc side. The current PR controller can reduce current ripple at twice line frequency effectively and track the reference sinusoidal waveform accurately. Meanwhile, the PR controller can reduce the grid current measurement errors. The analysis indicates that the PR controller stability mainly depends on proportion coefficient, resonant coefficient and cutoff frequency. Simulation results carried out on a 3.3kW single phase PWM rectifier model show the proposed PR control scheme can suppress the second-order ripple current in steady state effectively.

Copyright

Acknowledgements

The authors gratefully acknowledge the support from the Beijing Municipal Science and Technology Commission of China (Grant no. Z121100006612006).

References

[1] D. Sbordone, I. Bertini, B. Di Pietra, M. C. Falvo, A. Genovese and L. Martirano, "EV fast charging stations and energy storage technologies: a real implementation in the smart micro grid paradigm," in Electric power systems research, vol. 120, pp. 96-108, Mar. 2015.

[2] Hussain Shareef, Md. Mainul Islam and Azah Mohamed, "A review of the stage-of-the-art charging technologies, placement methodologies, and impacts of electric vehicles," in Renewable and sustainable energy reviews, vol. 64, pp. 403-420, Oct. 2016.

[3] S. Jaganathan and W. Gao, "Battery charging power electronics converter and control for plug-in hybrid electric vehicle," in *Vehicle power and propulsion conference*, pp. 440-447, 2009.

[4] X. Zhou, G. Wang, S. Lukic, S. Bhattacharya and A. Huang, "Multi-function bi-directional battery charger for plug-in hybrid electric vehicle application," in *ECCE*, pp. 3930-3936, 2009.

[5] S. Li, X. Wang, Z. Yao, T. Li and Z. Peng, "Circulating current suppressing strategy for MMC-HVDC based on nonideal proportional resonant controllers under unbalanced grid conditions," in *IEEE Trans. on power electron*., vol.30, no. 1, pp. 387-397, Jan. 2015.

[6] R. Teodorescu, F. Blaabjerg, M. Liserre and P. C. Loh, "Proportional-resonant controllers and filters for grid-connected voltage-source converter," in *IEE Proc.-Electr. Power appl.*, vol.153, no. 5, pp. 750-762, Sep. 2006.

[7] C. Xia, B. Ji and Y. Yan, "Smooth speed control for low-speed high-torque permanent-magnet synchronous motor using proportional-integral-resonant controller," in *IEEE Trans. on industrial electronics*., vol.62, no. 4, pp. 2123-2133, Apr. 2015.

[8] J. Wang, Y. Li, Y. Zheng and X. Yuan, "PIR-based control for three-phase PWM rectifier with H-bridge load," in *IPEMC*, pp. 1643-1647, Jan. 2009.

[9] V. Phan and H. Lee, "Performance enhancement of stand-alone DFIG systems with control of rotor and load side converters using resonant controllers," in *IEEE Trans. on industry applications*, vol.48, no. 1, pp. 199-210, Jan. 2012.

[10] X. Yuan, J. Chai and J. Wang, "DC-link voltage ripple reduction for a transformerless modular wind generator system," in *PEMD*, pp. 1-6, 2010.